Supplement of

Characterizing lead-rich particles in Beijing's atmosphere following coal-to-gas conversion: Insights from single particle aerosol mass spectrometry

Xiufeng Lian[1, 2], Yongjiang Xu[1], Fengxian Liu[3], Long Peng[4], Xiaodong Hu[5], Guigang Tang[6], Xu Dao[6], Hui Guo[7], Liwei Wang[8], Bo Huang[2], Chunlei Cheng[1], Lei Li[1], Guohua Zhang[9], Xinhui Bi[9], Xiaofei Wang[10], Zhen Zhou[1], Mei Li[1,*]

[1] College of Environment and Climate, Institute of Mass Spectrometry and Atmospheric Environment, Guangdong Provincial Engineering Research Center for On-line Source Apportionment System of Air Pollution, Jinan University, Guangzhou , 510632 PR China

[2] Guangzhou Hexin Instrument Co., Ltd., Guangzhou 510530, Guangdong, China

[3] Taiyuan University of Technology, Taiyuan 030024, PR China

[4] College of Ecology and Environment, Xin Jiang University, Urumqi 830046, PR China

[5] Jiangmen Laboratory of Carbon Science and Technology, Hong Kong University of Science and Technology (Guangzhou), Jiangmen 529100, PR China

[6] China National Environmental Monitoring Centre, Beijing 100012, PR China

[7] Hunan Province Environmental Monitoring Center, Changsha 410014, PR China

[8] Environment Emergency Monitoring and Accident Investigation Center, Jiaxing 314000, PR China

[9] State Key Laboratory of Organic Geochemistry and Guangdong Provincial Key Laboratory of Environmental Protection and Resources Utilization, Guangzhou Institute of Geochemistry, Chinese Academy of Sciences, Guangzhou 510640, PR China

[10] Department of Environmental Science and Engineering, Shanghai Key Laboratory of Atmospheric Particle Pollution and Prevention, Fudan University, Shanghai 200433, China

Correspondence to: limei@jnu.edu.cn

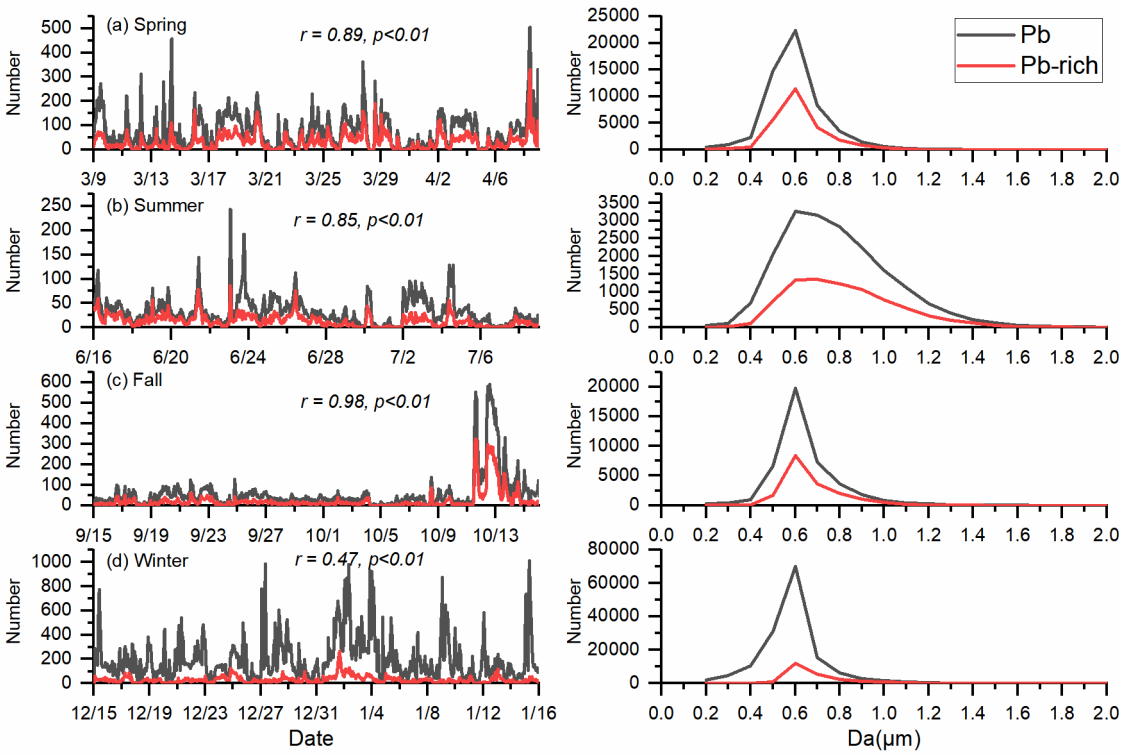

Figure S1. Time series and size distribution of Pb-containing particles and Pb-rich particles

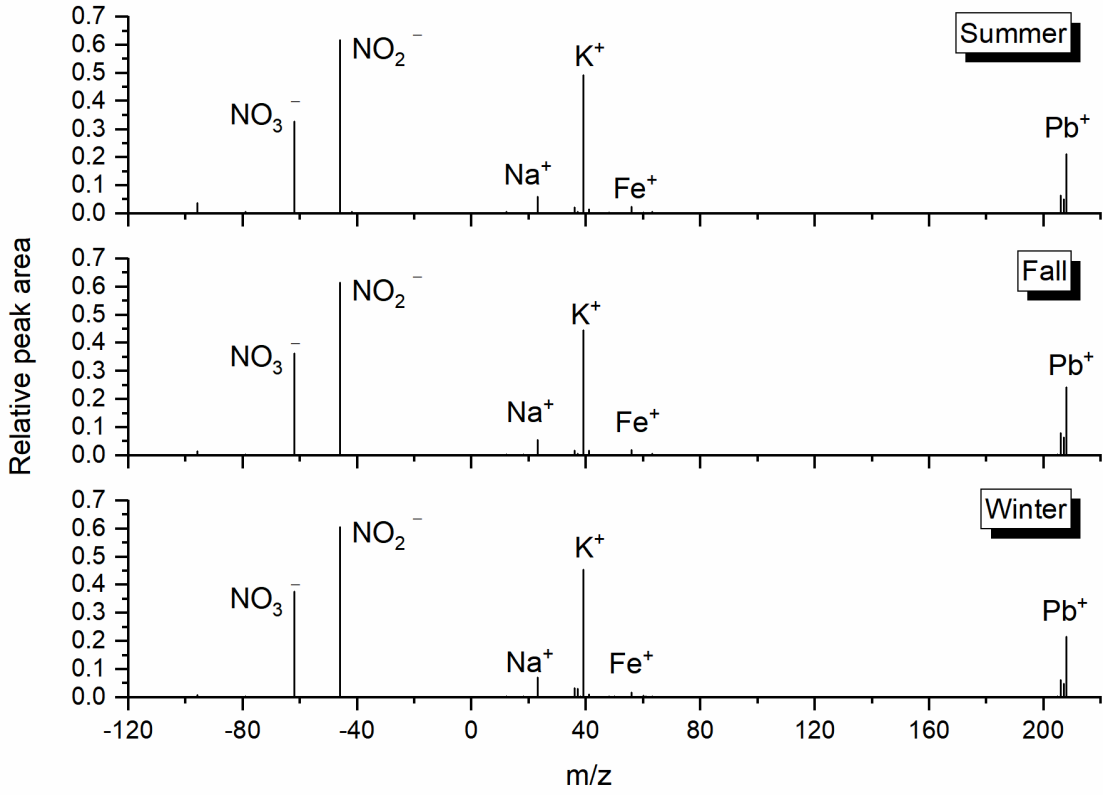

Figure S2. The average mass spectrum of Pb-N particles from summer to winter in 2019.

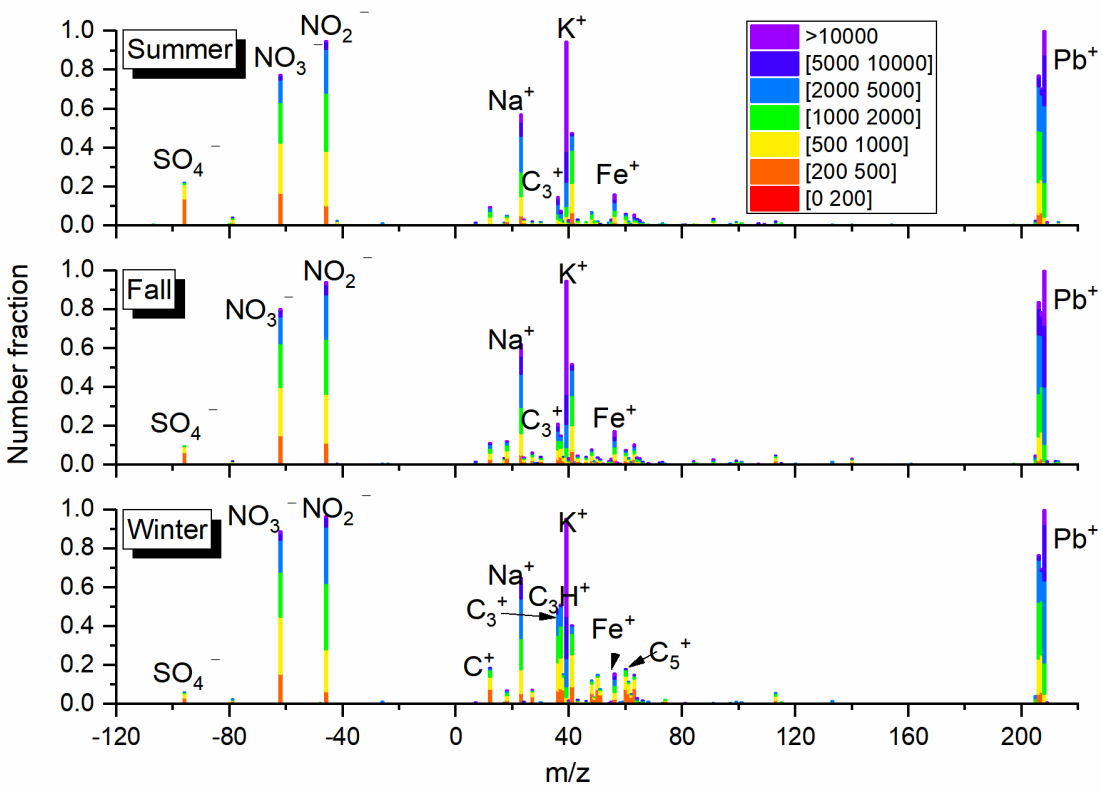

Figure S3. The digital spectrum of Pb-N particles from summer to winter in 2019.

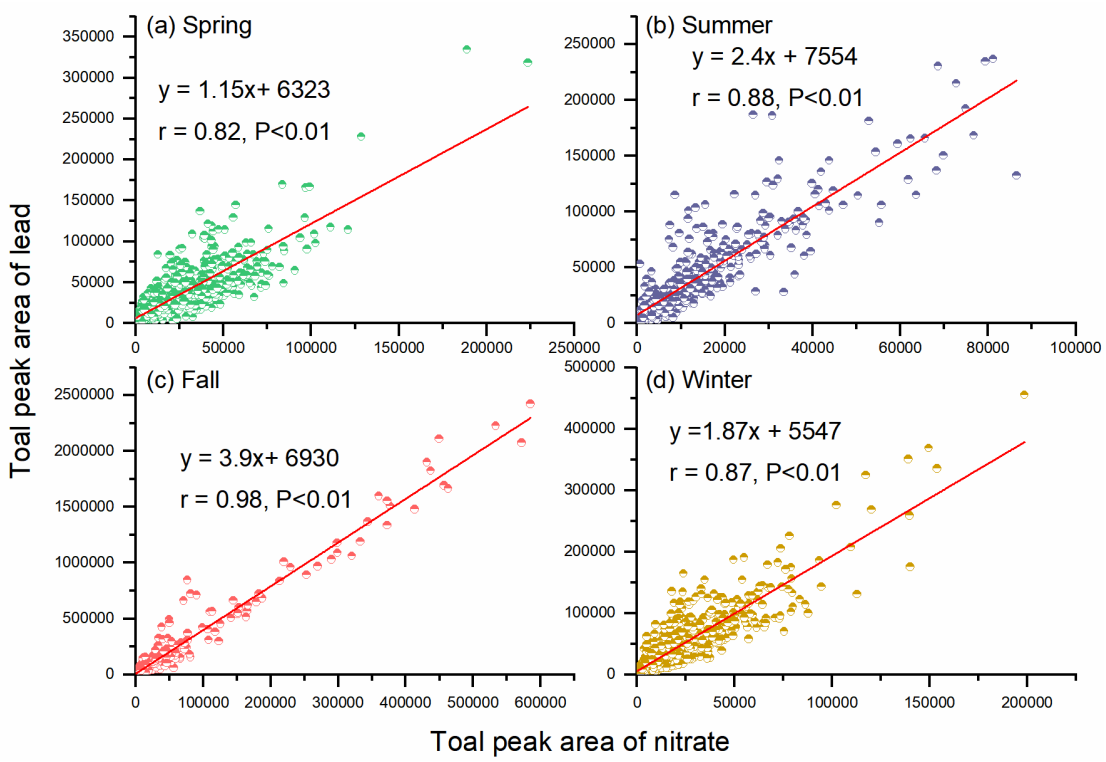

Figure S4. Correlation between the total peak area of nitrate (sum peak area of m/z −46 and −62) and the total peak area of lead (sum peak area of m/z 206, 207, and 208) in Pb-N particles.

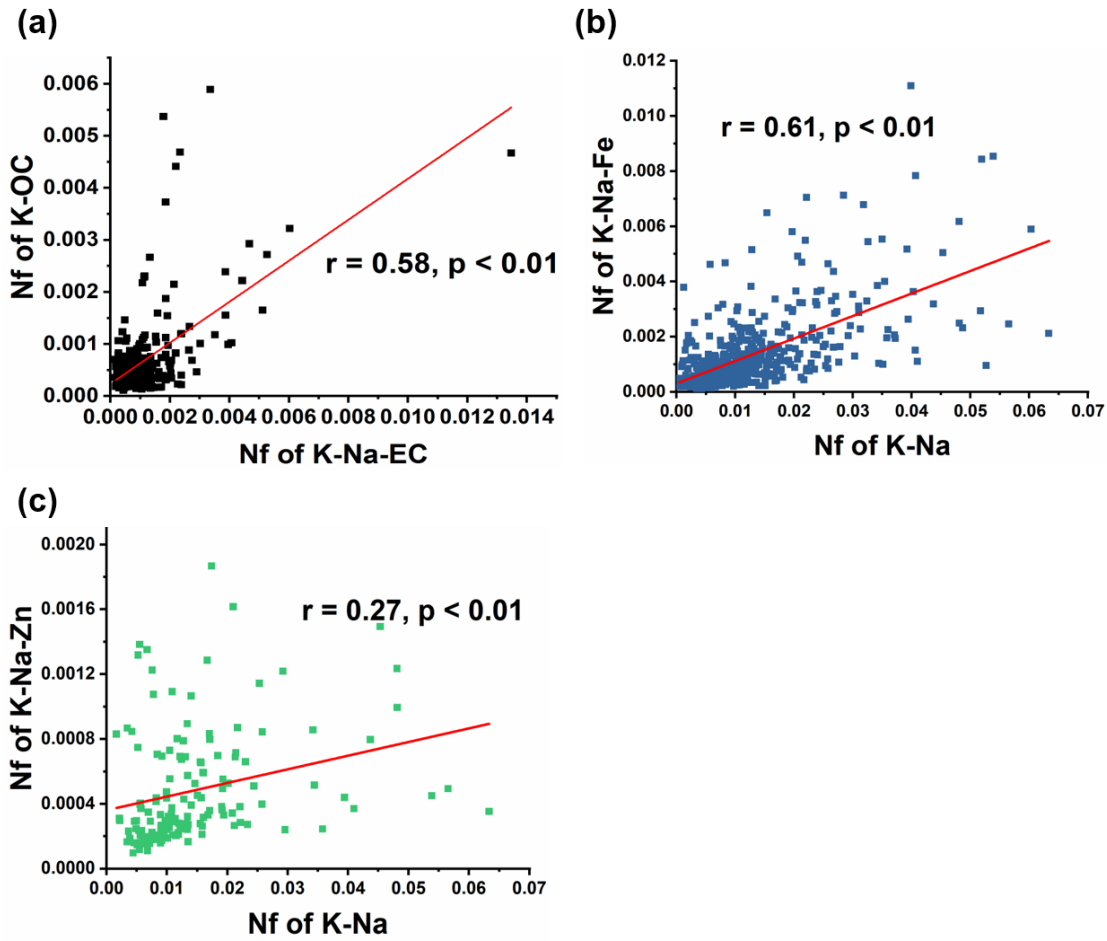

Figure S5. Correlation between the number fractions of K-Na-EC and KOC particles (a), K-Na and K-Na-Fe particles (b), K-Na and K-Na-Zn particles (c).

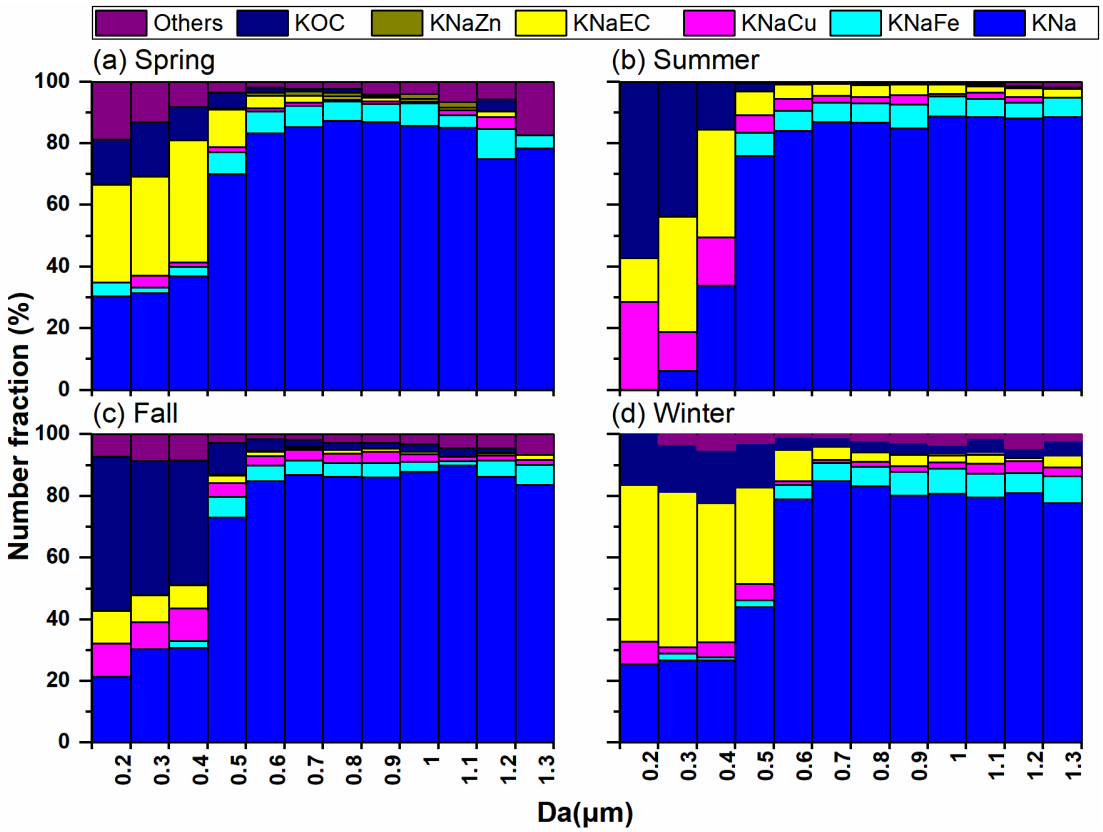

Figure S6. Number fractions for size distribution of the main Pb-rich particle types classified based on positive spectrum from spring to winter, respectively.

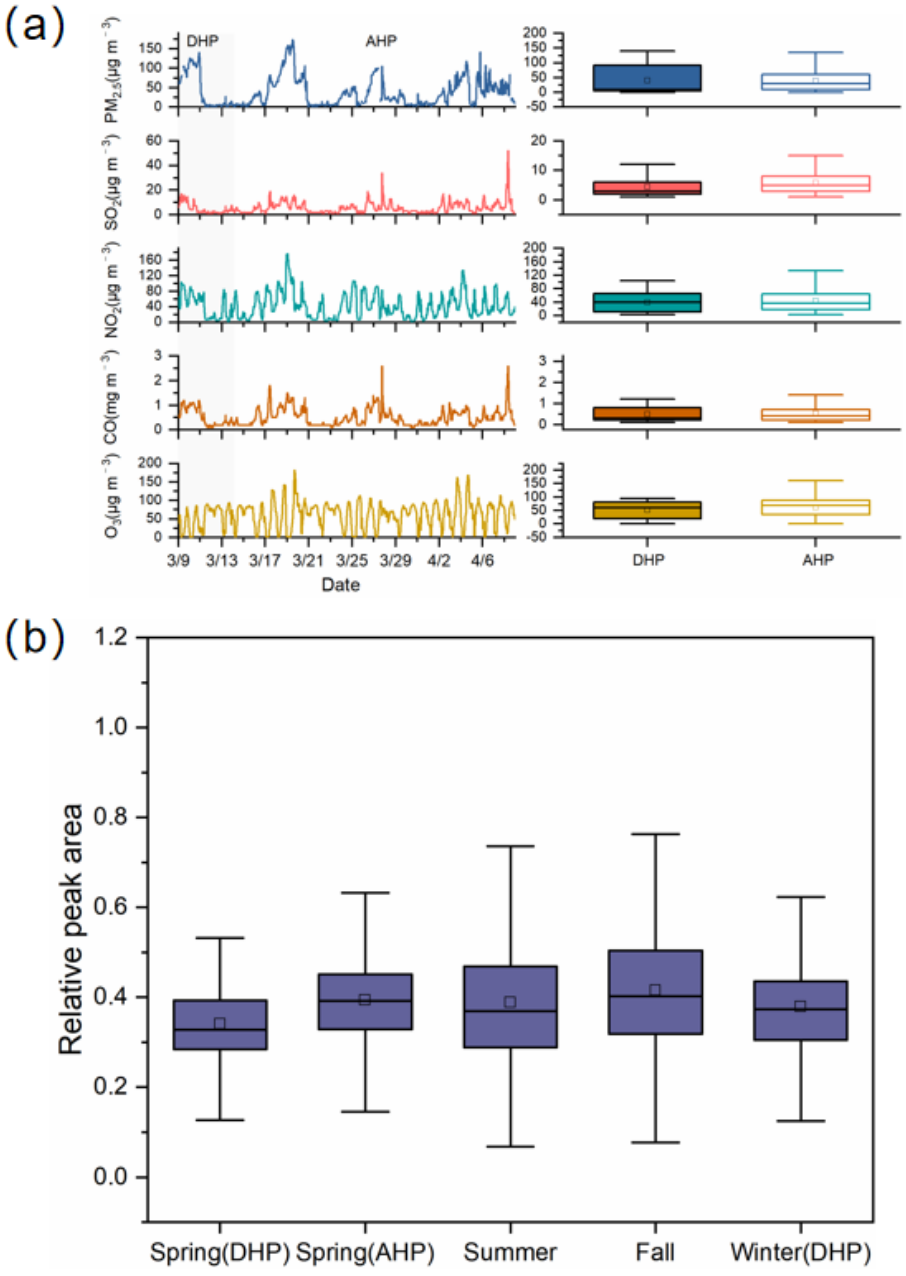

45 **Figure S7. (a) Time series of pollutant concentrations ($PM_{2.5}$, NO_2, SO_2, CO, and O_3) and box plots of pollutant concentrations during heating (DHP) and non-heating (AHP) periods during spring; (b) The relative peak area of Pb in Pb-rich particles during four seasons.**

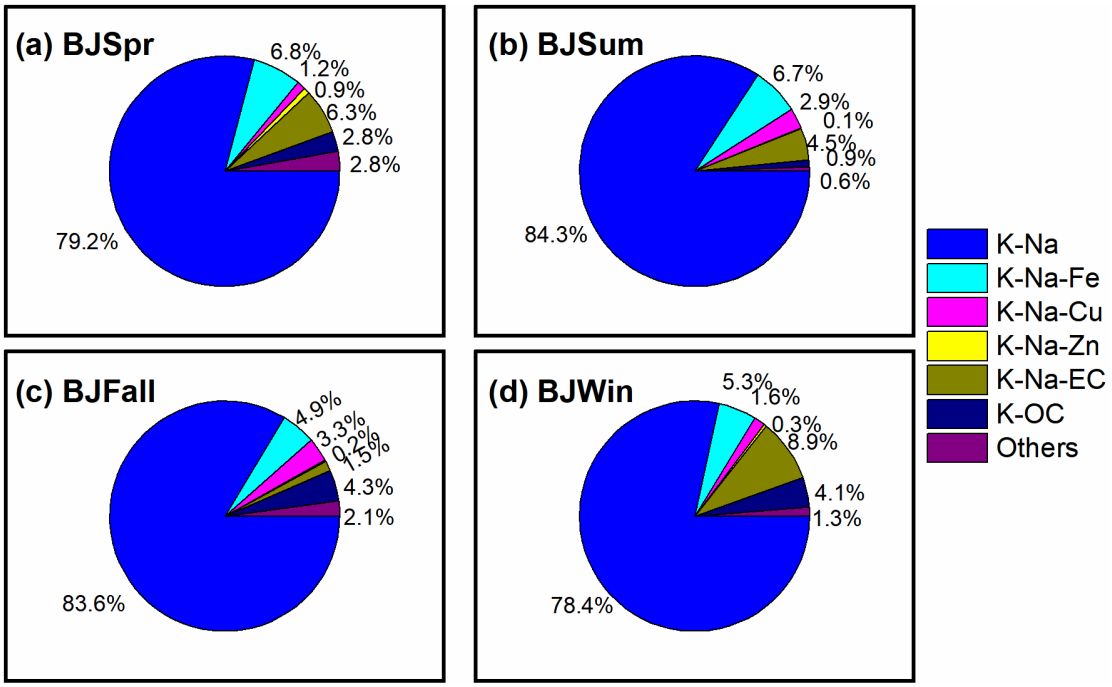

Figure S8. The number fractions of the main Pb-rich particle types from spring to winter in 2019.

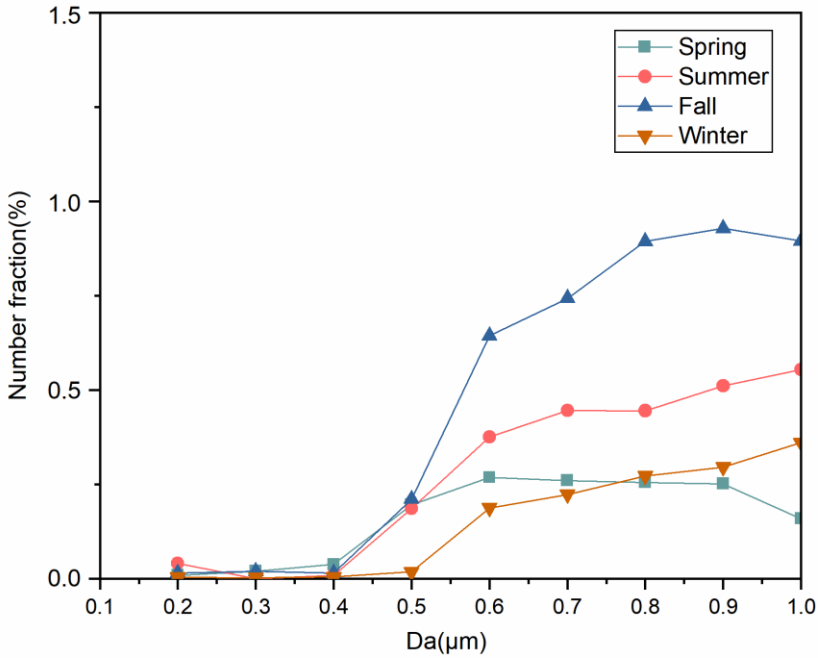

Figure S9. Number fractions for size distribution of Pb-N particles from spring to winter, respectively.

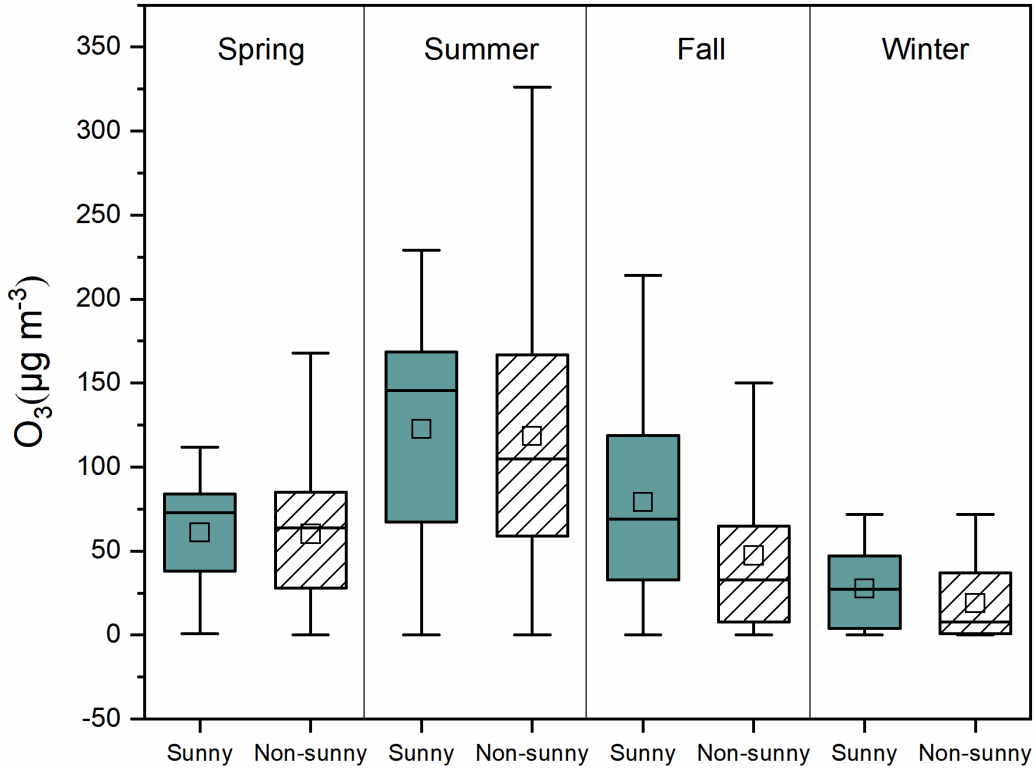

Figure S10. The ozone concentration on sunny and non-sunny days during four seasons.

55

Table S1 Average value and standard deviation of meteorological parameters and the concentration of pollutants during sampling periods.

Site	Date	SO_2	NO_2	O_3	$PM_{2.5}$	T	RH	WS
		($\mu g/m^3$)				（℃）	（%）	(m/s)
	9 Mar-8 Apr 2019	6 ± 5	45 ± 32	62 ± 37	41 ± 37	12 ± 5	29 ± 14	2 ± 2
	16 Jun-17 Jul 2019	4 ± 3	32 ± 19	119 ± 75	33 ± 21	27 ± 5	56 ± 19	2 ± 1
	15 Sep-16 Oct 2019	4 ± 4	41 ± 22	59 ± 56	35 ± 26	19 ± 6	61 ± 21	1 ± 1
	15 Dec 2019-15 Jan 2020	6 ± 5	49 ± 30	24 ± 23	36 ± 32	-1 ± 3	49 ± 20	2 ± 1